

## Microscopic current dynamics in nanoscale junctions

Na Sai,<sup>1,2</sup> Neil Bushong,<sup>1</sup> Ryan Hatcher,<sup>3</sup> and Massimiliano Di Ventra<sup>1</sup>

<sup>1</sup>*Department of Physics, University of California, San Diego, La Jolla, California 92093, USA*

<sup>2</sup>*Department of Physics, The University of Texas, Austin, Texas 78712, USA*

<sup>3</sup>*Department of Physics, Vanderbilt University, Nashville, Tennessee 37235, USA*

(Received 15 August 2006; revised manuscript received 7 January 2007; published 13 March 2007)

So far, transport properties of nanoscale contacts have been studied mostly within the static scattering approach. The electron dynamics and the transient behavior of current flow, however, remain poorly understood. We present a numerical study of microscopic current flow dynamics in nanoscale quantum point contacts. We employ an approach that combines a microcanonical picture of transport with time-dependent density-functional theory. We carry out atomic and jellium model calculations to show that the time evolution of the current flow exhibits several noteworthy features, such as nonlaminarity and edge flow. We attribute these features to the interaction of the electron fluid with the ionic lattice, to the existence of pressure gradients in the fluid, and to the transient dynamical formation of surface charges at the nanocontact-electrode interfaces. Our results suggest that quantum transport systems exhibit hydrodynamical characteristics, which resemble those of a classical liquid.

DOI: [10.1103/PhysRevB.75.115410](https://doi.org/10.1103/PhysRevB.75.115410)

PACS number(s): 72.10.-d, 73.63.Rt, 71.15.Mb

### I. INTRODUCTION

Recent experimental progress has enabled imaging of coherent current flow dynamics in quantum point contacts formed in semiconductor heterostructures.<sup>1-4</sup> These advances in experimental techniques open the possibility that current flow through atomic or molecular junctions will be eventually imaged and controlled. Understanding the microscopic electronic flow patterns can aid the design of novel electronic devices. However, very few theoretical studies of current dynamics in nanoscale systems are currently available. Indeed, among the recent theoretical studies of transport in nanoscale systems, much emphasis has been placed on the steady-state conduction properties,<sup>5-15</sup> whereas the transient behavior of the current remains an unexplored area.

Electronic transport in nanoscale junctions is usually formulated within the stationary scattering picture, such as the one due to Landauer,<sup>16</sup> in which the conduction is treated as a collection of scattering events. This stationary approach, widely used to study transport in mesoscopic and nanoscale systems, has led to considerable success in understanding current-related effects other than the conductance, including, e.g., noise, local heating, and current-induced forces.<sup>17</sup> It has helped our understanding of the microscopic current distribution as well.<sup>18,19</sup> Nevertheless, the stationary approach assumes that the system is already in a steady state, leaving the questions of how a steady current establishes itself and what other phenomena are related to the dynamical formation of steady states in a nanojunction unsolved.

The dynamical nature of the current flow is better addressed in a time-dependent approach than in the stationary one. Time-dependent or ac transport approaches have been previously introduced in mesoscopic conducting systems.<sup>20-24</sup> Recently, an increasing amount of effort has been directed toward developing *ab initio* time-dependent approaches for nanoscale systems.<sup>25-35</sup> One such method was developed to study the ac conductance using the time-dependent density-functional theory<sup>36</sup> (TDDFT) combined

with absorbing boundary conditions.<sup>26</sup> Other methods have been developed based on the Landauer scattering formalism of transport that employ open boundary conditions.<sup>27,29,31,32</sup>

More recently, a microcanonical formalism that treats electronic transport as a discharge across a nanocontact connecting two large but finite charged electrodes was introduced.<sup>25</sup> The formulation has been combined with TD-DFT to study the dynamical formation of quasisteady currents, local chemical potentials,<sup>30</sup> and electron-ion interactions.<sup>28</sup> This formalism would yield the exact total current flowing from one electrode to the other if the exact functional were known, regardless of whether the system achieves a steady state. In practice, in *ab initio* transport calculations, one only uses approximate forms of the functional such as the adiabatic local-density approximation (ALDA). It has been shown recently that the electronic correlation effect beyond the ALDA gives rise to additional resistance in molecular junctions.<sup>37-40</sup> The spurious self-interaction implicit in the ALDA further complicates calculations of the conduction properties.<sup>41-43</sup> The sensitivity of various transport properties to the suggested corrections remains only partially understood.

The dynamical establishment of a quasisteady current has been investigated by a number of authors.<sup>28-30,44</sup> It has been demonstrated that a quasisteady current can establish itself across a junction on a femtosecond time scale without the presence of inelastic scattering.<sup>30</sup> This is due to the geometrical “squeezing” experienced by the electrons crossing the nanojunction.<sup>25</sup> The conductance calculated from the microcanonical formula was shown to be in good agreement with that obtained from the static density-functional theory approach in prototypical atomic junctions<sup>28,30</sup> as well as in molecular junctions.<sup>45</sup> Nevertheless, a study of the microscopic behavior of the electron flow, and, in particular, of the current flow morphology in nanojunctions, is still lacking.

In this paper, we carry out real-time numerical simulations of current flow in metallic nanojunctions using the microcanonical formalism, where we employ TDDFT within the ALDA. We restrict the forthcoming discussion to the dy-

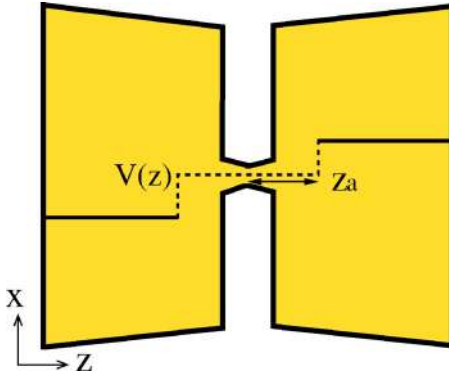


FIG. 1. (Color online) Sketch of the nanojunction geometry that is studied in the paper. At  $t < 0$ , a bias in the form of  $V(z) = V_0[H(z - z_a) - H(-z - z_a)]$  is applied to the junction (the central constriction is at  $z = 0$ ) such that the regions  $|z| > z_a$  bear a potential offset from the central constriction, where  $H(z)$  is the Heaviside step function.

namical behavior of electron and/or hole charges in the nanojunctions under the linear response regime, i.e., in which the bias is small and the current-voltage characteristics are linear. The paper is organized as follows. In Sec. II, we discuss model transport systems and numerical methods. In Sec. III, we present and discuss simulations of current dynamics in jellium and atomic junctions. We also analyze the effects of hydrodynamic pressure and electrode surface charges on the dynamics of the flow. In Sec. IV, we summarize the main conclusions of our work.

## II. MODEL AND METHODS

The nanoscale junction geometry studied in this paper is illustrated in Fig. 1. A narrow constriction separates two large but finite electrodes. We begin the simulations by applying a step-function-like electric bias across the junction such that the two electrodes bear equal and opposite potentials offset relative to the potential at the center of the junction. The distance from the bias discontinuity to the center of the junction is  $z_a$  (see Fig. 1). This bias induces a charge imbalance between the two sides of the system. At  $t = 0$ , we remove the bias and a discharge through the nanojunction ensues. The Kohn-Sham initial state therefore corresponds to the ground state of the Hamiltonian in the presence of the bias. Here, we are interested in the transient behavior during the phase in which the current is in the process of establishing a quasi-steady-state and immediately thereafter, i.e., long before the electrons that have passed through the constriction have had a chance to reach the far boundary of the electrodes.

To separate the effects of the electrons and of the atomic lattice, we have carried out calculations using a jellium model and an atomic model. In the jellium calculations, the electrodes are represented by two large jellium slabs 2.8 Å thick. The contact is a rectangular jellium block 2.8 Å wide and as thick as the electrodes. The distance between the jellium electrodes is 9.8 Å. In the atomic calculations, the junction is represented by two planar arrays of gold atoms sand-

wiching a single gold atom. We employ TDDFT and solve the effective single-particle Schrödinger equation

$$i\hbar \psi(\vec{r}, t) = \left[ -\frac{\hbar^2 \nabla^2}{2m} + V_{\text{eff}}(\vec{r}, t) \right] \psi(\vec{r}, t), \quad (1)$$

where the effective potential is given by

$$V_{\text{eff}}(\vec{r}, t) = V_{\text{ext}}(\vec{r}, t) + \frac{e^2}{2} \int \frac{n(\vec{r}', t)}{|\vec{r} - \vec{r}'|} d\vec{r}' + V_{\text{xc}}(\vec{r}, t). \quad (2)$$

The term  $V_{\text{xc}}(\vec{r}, t)$  is the exchange-correlation potential calculated within the adiabatic local-density approximation. The external (ionic) potential is modeled using pseudopotentials for the atomic calculations,<sup>46</sup> while in the jellium model, it is a local operator related to the uniform positive background jellium density  $\rho_0$  via  $V_{\text{ext}}(\vec{r}) = \frac{e^2}{2} \int \frac{n_0}{|\vec{r} - \vec{r}'|} d\vec{r}'$ , where  $n_0$  is equal to  $(\frac{4\pi r_s^3}{3})^{-1}$  inside the jellium and zero outside, and  $r_s$  is the Wigner-Seitz radius. In the jellium model, we choose  $r_s = 3a_B$  ( $a_B = \text{Bohr radius}$ ), which gives a good representation of bulk gold (see also discussion below). A “free-space” boundary condition is implemented such that the long-range potential is constructed only from the densities in the supercell<sup>47</sup>; that is, the system is not periodic. Additional numerical details can be found in the Appendix. The single-particle time-dependent current density is calculated via

$$\vec{j}(\vec{r}, t) = \sum_n \frac{\hbar}{2mi} [\psi_n^*(\vec{r}, t) \vec{\nabla} \psi_n(\vec{r}, t) - \nabla \psi_n^*(\vec{r}, t) \psi_n(\vec{r}, t)], \quad (3)$$

where  $\psi_n$  denotes individual Kohn-Sham single-particle states. Note that in TDDFT the current density is not necessarily exact even if one calculates it with the exact functional (via the continuity equation, only the divergence of the current density would be exact). One would need to resort to time-dependent current density-functional theory<sup>48</sup> (TD-CDFD) to obtain the exact current density (with the exact functional). Nonetheless, due to the small viscosity of the electron liquid, we have found that the current density one obtains by using TDDFT within the ALDA and the one obtained by TDCDFD within the Vignale-Kohn functional<sup>48</sup> are qualitatively similar.<sup>49</sup>

Even if the contact between the electrodes were removed, the current between the two electrodes would not completely vanish because of quantum tunneling. This bare tunneling current can conveniently be used to compare the jellium and the atomic calculations. The jellium edges are placed at half the interplanar spacing of the lattice.<sup>50</sup> This way, the jellium model and the pseudopotential calculations both yield tunneling current densities of  $\sim 0.05 \mu\text{A}/\text{\AA}^2$  at a bias of 0.2 V. The agreement indicates that the jellium model is a good representation of two large metal electrodes. This is consistent with the results of previous density-functional calculations.<sup>51</sup>

## III. RESULTS AND DISCUSSION

### A. Flow dynamics through jellium model junctions

In a nanojunction such as an atomic point contact, the dimensions of the leads are usually much larger than those of

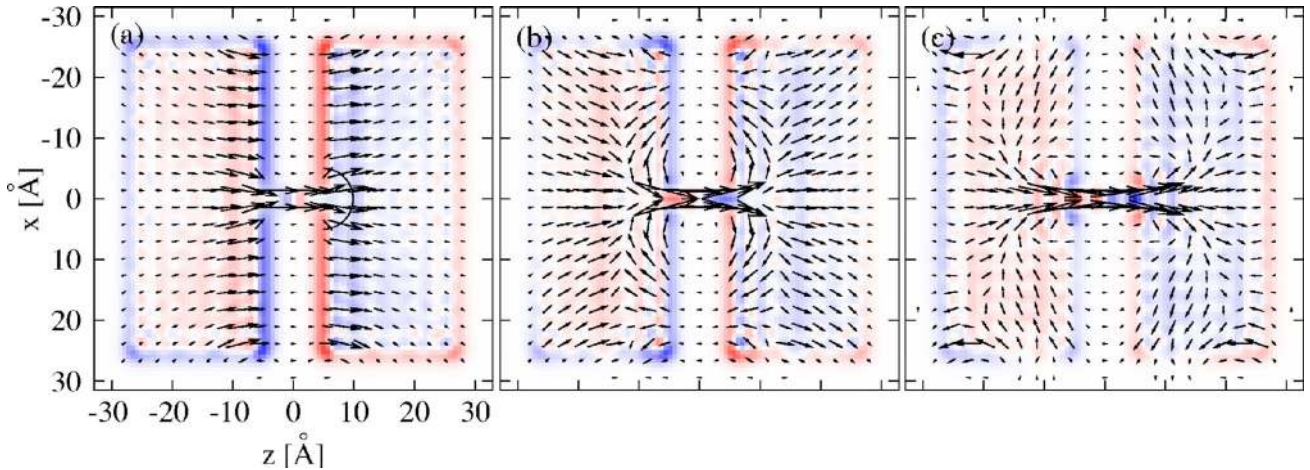


FIG. 2. (Color online) Current flux for a series of times in a nanoscale quantum point contact system in the jellium model. The applied bias at  $t < 0$  is  $\Delta V = 0.2$  V. The field lines in each panel depict the direction and amplitude of the current density vectors, while the colors give extra electron (red) or hole (blue) density: (a)  $t = 0.4$  fs, (b)  $t = 0.8$  fs, and (c)  $t = 1.6$  fs. In (a), the semicircle marks the contour along which the radial component of the current density is calculated (see text and Fig. 3).

the central constriction. In addition, not far from the contact, we expect the electron momentum to converge to the value characteristic of the bulk leads. Therefore, the momentum of an electron coming from the leads and entering the contact has to change considerably. This gives rise to resistance, and for a truly nanoscale junction, this momentum mismatch is mainly responsible for the establishment of quasi-steady-states.<sup>25,30,52</sup> Using the above dynamical approach, we can now study how this translates into microscopic current flow through the nanocontact and into the leads by calculating the current density at different times.

To begin, we follow the method described in the preceding section to impose a charge imbalance in the jellium model system. A discussion of the effect of the lattice on the flow dynamics will be presented in the following section. The initial bias is chosen such that the discontinuity happens at the edge of the jellium slab near the central constriction (i.e.,  $z_a \cong 5$  Å). The flow pattern is independent of the location of the discontinuity once the current starts to flow through the center of the junction. In Fig. 2, we plot three snapshots of the current density to illustrate the evolution of the flow. Due to the bias offset near the jellium edges, a dipolar layer forms on each of the two contact-electrode interfaces. As a result, the initial current flow is uniform on both sides as shown in Fig. 2(a). Very little current flows in the nanojunction at this point, however, the current steadily rises. In Fig. 2(b), the current density becomes convergent toward the center of the nanojunction. Interestingly, as the excess charge from the left electrode reaches the contact, there is a period of adjustment during which the dominant flow is in the lateral direction, i.e., parallel to the facing surfaces of the electrodes.

To quantify the evolution of the angular distribution of the electron flow, in Fig. 3 we plot a time series of the radial component of the current density along a semicircle contour centered on the junction as a function of the angle on the semicircle [see Fig. 2(a)]. One can see that initially a “wave” of excess charge approaches the nanocontact. Then, the radial current density peaks at very large angles ( $\sim \pm 75^\circ$ ), i.e.,

the current density near the contact is dominated by the flow along the electrode edges in the lateral direction. The peaks then gradually move toward the central axis, and the current density adjusts to a more “focused” pattern as shown in Fig. 2(c). We have also examined a junction consisting of a jellium circular “island” between the electrodes. We have observed edge flow in this case as well. The edge flow is not a quantum interference pattern and cannot be compared with the fringes observed in the two-dimensional (2D) electron gas quantum point contacts.<sup>4</sup> Instead, we suggest that the flow pattern is controlled by hydrodynamic effects and forces due to surface charges. We analyze these in Sec. III C.

The structure of the current density is analogous to a classical fluid flowing across a narrow constriction. This is not surprising because an inhomogeneous electron system can be, indeed, characterized by a set of hydrodynamical relations expressed in terms of the particle density and velocity field.<sup>53–56</sup> More recently, in particular, a hydrodynamical approach was proposed for nanoscale transport systems,<sup>55</sup> further strengthening the analogy between the dynamics of the electron liquid and the one of a classical liquid. We note that the present calculations do not take into account the physical

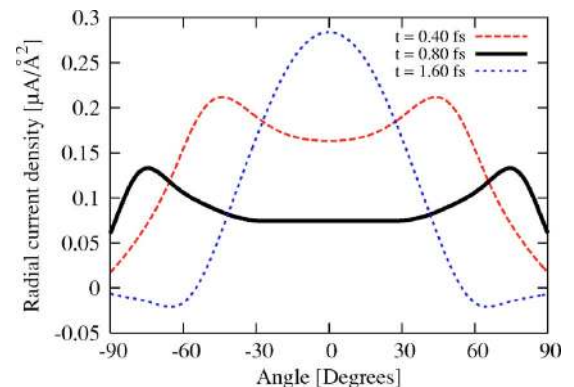


FIG. 3. (Color online) Time series of the radial amplitude of the current densities along a semicircle of radius 3 Å centered on the nanojunction, as a function of angle along the contour.

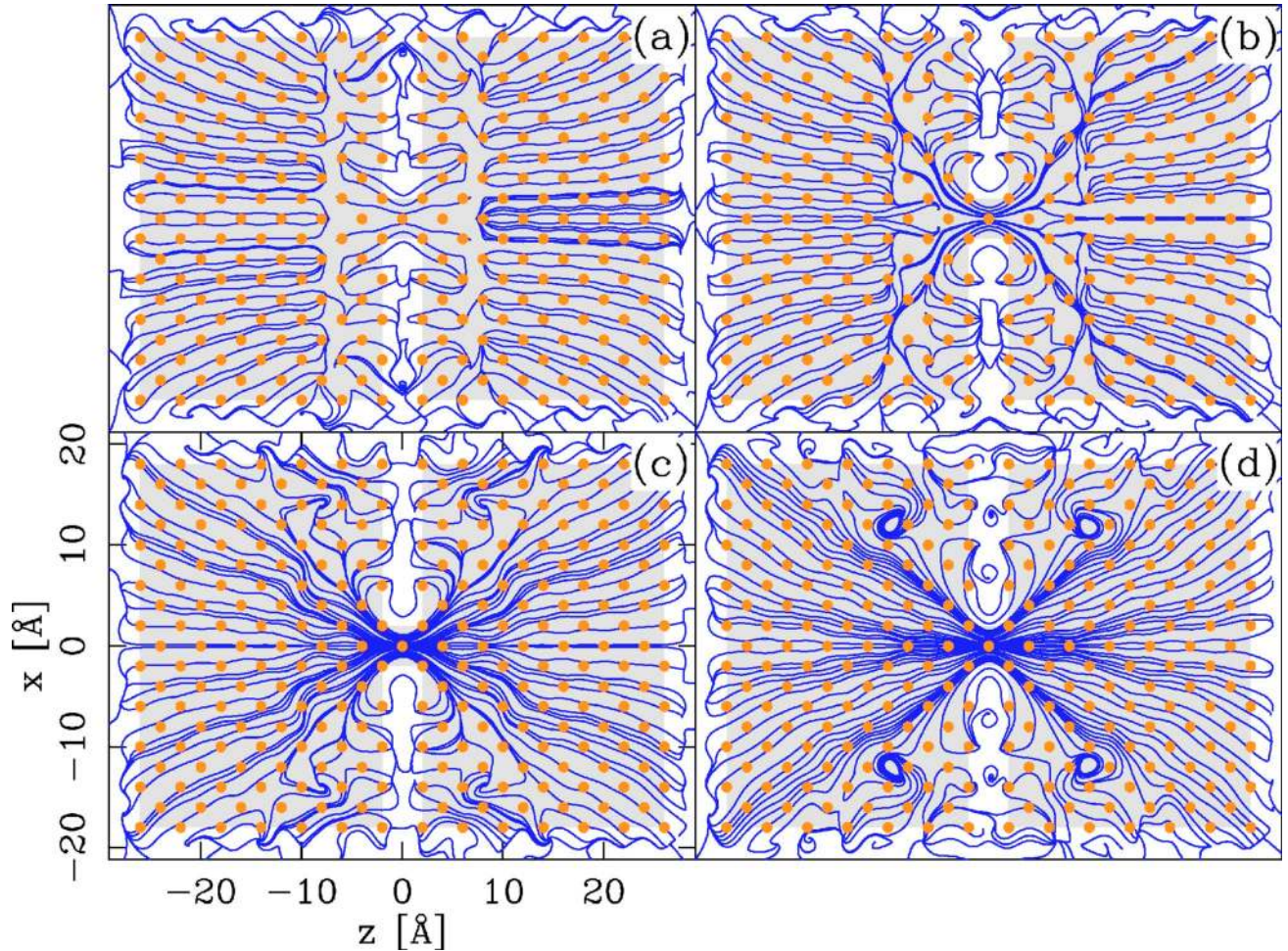


FIG. 4. (Color online) Time sequence of electron current streamlines in the atomic junction described in Sec. II. (a)–(d) correspond to  $t=0.2, 0.25, 0.3,$  and  $0.35$  fs, respectively. The dots denote atomic sites that correspond to the (001) facets of the gold fcc lattice. The applied bias at  $t < 0$  is  $\Delta V=0.2$  V.

viscosity of the electron liquid.<sup>56,57</sup> An inviscid fluid can therefore be used as a model for the dynamical behavior of the present electron liquid.

### B. Flow dynamics through atomic junctions

The jellium model was a convenient way to probe the microscopic current dynamics in an electron gas. To understand the influence of the lattice on the flow, we carried out simulations that included an ionic background modeled by pseudopotentials. The atomic calculations were carried out for 2D gold nanojunctions and were initialized in the same way as the jellium calculations. The theoretical and experimental conductances are in very good agreement for this system.<sup>58</sup> We chose lattice arrangements that correspond to the (001) and (111) facets of the gold fcc lattice [the dots in Fig. 4 represent the atomic sites for the (001) configuration].

Electric current streamlines at different times in the simulation are plotted in Figs. 4(a)–4(d). The streamlines are calculated by integrating the current-density field upstream and downstream,  $d\vec{r}/ds = \pm \vec{j}(\vec{r}(s))$ . The morphology of the current flow in the atomic junction and in the jellium model is

remarkably similar,<sup>59</sup> indicating that the jellium model is a good representation of the gold electrodes. Nevertheless, a number of different features appear in the atomic calculations.

Figure 4(c) shows that once a steady flow through the junction is established, the current spreads into a wedge-shaped region inside the electrodes. The flow morphology for each of the two different lattice arrangements is similar except that the flow spreads over a broader wedge-shaped region in the (111) lattice. Another common feature in the atomic calculations is the presence of a stagnant zone at the corner of the electrode boundary. There is little current flow into or out of this zone. This is similar to a classical fluid where a stagnant zone can sometimes be located at the entrance or exit of a channel.

One profound difference between the atomic and the jellium calculations is the formation of eddies evident in the former but not in the latter. In the jellium calculations carried out within the linear-response bias regime, the current flux lines are laminar. In contrast, in the atomic calculations, the eddies appear as localized circular flow that can be observed in Fig. 4(d). The eddies develop in both electrodes and the size of the eddies is comparable to the interatomic distance.

The eddies are reminiscent of the vortices that form in a classical fluid at higher Reynolds number when the fluid encounters obstacles. As is well known, vortices can also occur when velocity shear is present within a continuous fluid (Kelvin-Helmholtz instability). We suggest that the lattice ionic obstacles and the boundaries separating the flow zone and the stagnant zone facilitate the formation of the observed eddies in our simulations.

The formation of current vortices has been previously reported in 2D ballistic quantum billiards.<sup>60,61</sup> In these quantum systems, a rich variety of flow patterns ranging from regular to chaotic is possible.<sup>62</sup> While we cannot draw direct analogies with these open and mesoscopic transport systems, an unstable and turbulent flow has been recently predicted in nanoscale systems.<sup>55</sup> We have argued that the ALDA electron liquid in our simulations corresponds approximately to an inviscid fluid. We therefore suggest that in the presence of a lattice, hydrodynamical instabilities or turbulence can occur in nanotransport systems even in the absence of a physical viscosity.

### C. Hydrodynamics and the formation of surface charges

To understand what drives the edge flow along the electrode surfaces, we examine the evolution of the charge distribution near the surfaces of the junction. For this purpose, we apply a step-function bias such that the potential discontinuity in each electrode occurs at  $z_a \cong 10 \text{ \AA}$ , which cuts across the electrode, as illustrated in Fig. 1. In Fig. 5(a), we plot a time series of the  $x$ - $y$  plane-averaged excess charge density along the  $z$  axis. At  $t=0$ , two symmetric dipolar layers form inside the electrodes as a result of the bias offsets. As the current starts to flow through the contact and gradually reaches a quasi-steady-state, a global charge redistribution becomes apparent. The dipolar layers gradually vanish and are replaced by surface charge layers that form at the contact-electrode interfaces. The charge contour plots of Figs. 5(b) and 5(c) further illustrate the formation of surface charges as a result of current flow.

The formation of surface charges around the central constriction is reminiscent of the formation of residual-resistivity dipoles introduced by Landauer.<sup>16</sup> It has been suggested that a continuous current flow arriving at a junction must be accompanied by self-consistently formed charges at the electrode surfaces.<sup>51</sup> The effect should be taken into account to correctly characterize the electrostatic potential and the nonequilibrium conducting properties in a transport calculation.<sup>63</sup> In this work, we provide a numerical demonstration of the dynamical formation of these surface charges using a time-dependent approach.

We have already observed that, as the surfaces of the electrodes are populated by excess charges, a lateral flow starts to develop along the surfaces. This behavior is illustrated in Fig. 3, where the radial current flux at  $t=0.8 \text{ fs}$  shows two pronounced peaks at very large angles. We attempt to interpret this behavior within the framework of an effective classic hydrodynamic model of an inviscid charged fluid. The acceleration of the fluid is then given by Euler's equation  $\partial \vec{v} / \partial t + (\vec{v} \cdot \nabla) \vec{v} = -\vec{\nabla} P / m_e n - e \vec{\nabla} \varphi / m_e$ , where  $\vec{v}$  is the fluid ve-

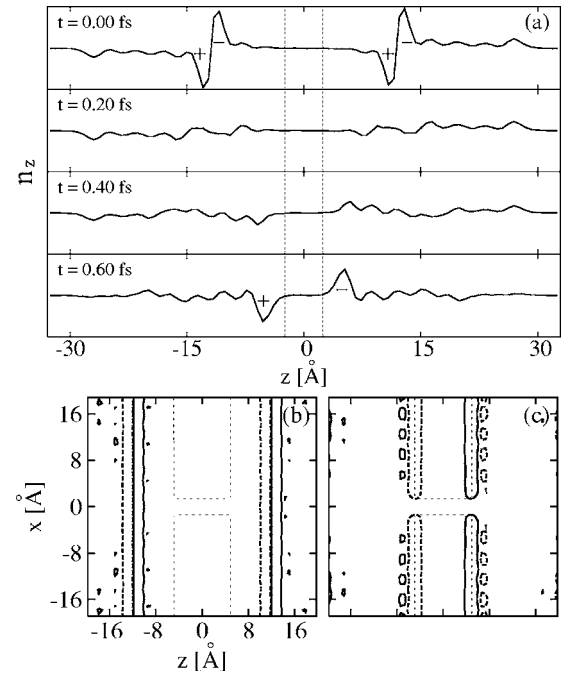


FIG. 5. (a) Planar averaged charge density from  $t=0$  to  $t=0.6 \text{ fs}$  for a jellium junction. The change in the peaks indicates the dynamic process in which excess charge builds up at the surfaces. The sign of the surface charges indicates that electron charges accumulate on the right and hole charges on the left. [(b) and (c)] Excess charge in the vicinity of the contact at  $t=0$  and  $t=0.6 \text{ fs}$ . The thick solid lines indicate excess electrons, while thick dashed lines indicate excess holes. The thin dashed lines mark the edges of the jellium electrodes and the contact.

locity,  $n$  is the fluid particle density,  $m_e$  is the electron mass, and  $\varphi$  is the electrostatic potential. The first term on the right-hand side is the acceleration due to a gradient in electron pressure. The second term is the acceleration due to the electric field of the excess charges on the surfaces of the electrode. The electric field drives the electrons and/or holes toward the surfaces to cancel out the excess charges.

The inertial term in the above equation can be estimated as  $|(\vec{v} \cdot \nabla) \vec{v}| \sim v^2 / L \sim 10^6 \text{ m}^2 / \text{s}^2 L^{-1}$ . Here,  $L$  denotes the characteristic length scale over which we expect a departure from uniform flow, so that  $\nabla \sim L^{-1}$ . Velocity of the flow in the simulation reaches  $v \sim 10^3 \text{ m/s} \ll v_F$ , where  $v_F \approx 1.4 \times 10^6 \text{ m/s}$  is the Fermi velocity of bulk gold. The hydrodynamical pressure can be calculated from the derivative of the ground-state energy with respect to  $r_s$ ,  $P/n = -(r_s/3) \epsilon'(r_s)$ , where  $\epsilon(r_s)$  is the energy per particle.<sup>64</sup> Therefore,  $|\vec{\nabla} P| / m_e n \sim (1/5) v_F^2 |\vec{\nabla} n| / n$ . Here, we included only the ground-state energy of a noninteracting electron gas,  $\epsilon_0(r_s) = \frac{3}{5} \epsilon_F$ .<sup>65</sup> Let  $\delta n$  denote the change of the particle density as a result of the current or the formation of the surface charges. For the present junctions at these biases, we find that typically  $\delta n / n \leq 0.01$ . Then, the acceleration due to the pressure gradient is

$$|\vec{a}_P| = \frac{|\vec{\nabla} P|}{m_e n} \sim \frac{1}{5} \frac{v_F^2}{L} \frac{\delta n}{n} \approx 3 \times 10^9 \frac{\text{m}^2}{\text{s}^2} L^{-1}. \quad (4)$$

To estimate the magnitude of the electrostatic acceleration, we treat the layer of charge induced on the facing surfaces of the electrodes [as illustrated in Fig. 5(c)] as an infinite uniformly charged wire. The electric field of the wire is given by  $|\vec{\nabla}\varphi|=\lambda/2\pi\epsilon_0L$ ,<sup>66</sup> where  $\lambda$  is the linear density of excess charge,  $L$  is the distance to the wire, and  $\epsilon_0$  is the vacuum permittivity. The linear charge-density is calculated by averaging the charge-density difference  $e\delta n$  between the configuration with and without the current flow over the layer in which the charge accumulated at the contact-electrode interfaces. For the same junctions, we find  $\lambda\sim 0.016\text{ e}/\text{\AA}$ . The acceleration of charges due to this electric field can be calculated as

$$|\vec{a}_{el}|=\frac{e}{m_e}\frac{\lambda}{2\pi\epsilon_0L}\sim 5\times 10^{11}\frac{\text{m}^2}{\text{s}^2}L^{-1}. \quad (5)$$

These crude estimates imply that over the same distance  $L$ ,

$$|(\vec{v}\cdot\vec{\nabla})\vec{v}|\leq|\vec{a}_p|\leq|\vec{a}_{el}|, \quad (6)$$

which suggests that the hydrodynamic pressure gradients dominate over the inertia of the fluid (the flow is subsonic and compressible), while the maximum electrostatic force due to the surface charges is comparable to or larger than the pressure gradient force before the surface charge has been passivated. Therefore, it is plausible that the lateral flow observed in the simulation is primarily of electrostatic origin. In different junction geometries or in a different conductance regime, the ordering in Eq. (6) may be different.

We have also carried out a similar simulation using a parabolically shaped constriction that resembles a quantum point contact in the 2D electron gas. At a similar bias as in the nonparabolic junctions, we find similar surface charge accumulation along the boundaries of the electrodes in the vicinity of the contact. We believe that the analysis we have provided on the surface charge formation applies to this case as well. To the best of our knowledge, the accumulation of the surface charges has not been reported in adiabatic quantum point contacts before. It would thus be interesting to develop experimental techniques to explore the surface region of the quantum point contact in a 2D electron gas and the charge accumulation that we observe in our simulations.

#### IV. CONCLUSIONS

In this paper, we have used the microcanonical approach<sup>25</sup> to study the time-dependent current flow morphology and the charge distribution in discharging nanojunctions represented by both a jellium model and pseudopotentials. We have shown that the electron flow in the nanojunctions exhibits hydrodynamic features analogous to a classical fluid. We have found that in the atomic case, the current flow evolves into a wedge-shaped pattern flanked by stagnant zones. The flow develops nonlaminar features including eddy currents.

We suggest that the ionic lattice at the junction plays the role of ‘‘obstacles’’ in the dynamics of the electron liquid, with consequent development of these features. We have also demonstrated that excess surface charges accumulate dynamically along the electrodes. In addition, we have observed that for a period of time, there is strong current flow in the transverse direction. By employing an order-of-magnitude argument, we suggest that this flow is driven by both hydrodynamic forces due to the electron pressure and electrostatic forces due to the surface charge distributions. The latter forces dominate the initial dynamics in the junctions at hand.

The present study and a previous study<sup>30</sup> demonstrate that the microcanonical approach combined with time-dependent density-functional theory can be used to probe the transient behavior of the current in nanojunctions such as atomic-scale point contacts or molecular junctions.<sup>45</sup> The present approach supplements existing methods that are based on the static scattering picture and provides another tool to study relatively unexplored nanoscale transport phenomena from first principles.

The flow patterns we observe in metallic nanojunctions can be generalized to a number of other systems, such as molecular junctions, although many details may vary. In view of the recent advances in microscopic imaging techniques of coherent current flow in quantum point contacts in a 2D electron gas,<sup>4</sup> we hope that new experimental work exploring the behavior of current flow in atomic contacts and molecular junctions would soon emerge to supplement our studies.

#### ACKNOWLEDGMENTS

The work was supported by the Department of Energy Grant No. DE-FG02-05ER46204.

#### APPENDIX: NUMERICAL DETAILS

We performed time-dependent density-functional calculations using the program SOCORRO (Ref. 46) and an in-house program which implements TDDFT within the jellium model. The gold ions were modeled by norm-conserving Hamann pseudopotentials with 6s electrons as valence electrons.<sup>67</sup> We used the Perdew-Zunger local-density approximation exchange-correlation functional.<sup>68</sup> The atomic calculation employed a plane-wave basis set with an energy cutoff of 204 eV, which corresponds to a grid spacing of 0.2 Å. The energy eigenvalues vary by less than 1% by increasing the cutoff by 66%. In the jellium case, the calculations were performed using a real-space basis set where the space is uniformly discretized and the grid spacing is 0.7 Å. The eigenvalues vary by less than 3% by decreasing the grid spacing by 66%. The time evolution operator is represented using the Chebyshev method,<sup>69</sup> with a time step of  $5\times 10^{-4}$  fs in the atomic case and  $5\times 10^{-3}$  fs in the jellium case.

- <sup>1</sup>B. G. Briner, R. M. Feenstra, T. P. Chin, and J. M. Woodall, *Phys. Rev. B* **54**, R5283 (1996).
- <sup>2</sup>M. A. Eriksson, R. G. Beck, M. Topinka, J. A. Katine, R. M. Westervelt, K. L. Campman, and A. C. Gossard, *Appl. Phys. Lett.* **69**, 671 (1996).
- <sup>3</sup>R. M. Feenstra and B. R. Briner, *Superlattices Microstruct.* **23**, 699 (1998).
- <sup>4</sup>M. A. Topinka, B. J. LeRoy, S. E. J. Shaw, E. J. Heller, R. M. Westervelt, K. D. Maranowski, and A. C. Gossard, *Science* **289**, 2323 (2000).
- <sup>5</sup>E. G. Emberly and G. Kirczenow, *Phys. Rev. B* **58**, 10911 (1998).
- <sup>6</sup>M. Di Ventra, S. T. Pantelides, and N. D. Lang, *Phys. Rev. Lett.* **84**, 979 (2000).
- <sup>7</sup>Y. Xue, S. Datta, and M. A. Ratner, *J. Chem. Phys.* **115**, 4292 (2001).
- <sup>8</sup>J. Taylor, H. Guo, and J. Wang, *Phys. Rev. B* **63**, 245407 (2001).
- <sup>9</sup>P. S. Damle, A. W. Ghosh, and S. Datta, *Phys. Rev. B* **64**, 201403(R) (2001).
- <sup>10</sup>M. Brandbyge, J.-L. Mozos, P. Ordejón, J. Taylor, and K. Stokbro, *Phys. Rev. B* **65**, 165401 (2002).
- <sup>11</sup>J. Heurich, J. C. Cuevas, W. Wenzel, and G. Schön, *Phys. Rev. Lett.* **88**, 256803 (2002).
- <sup>12</sup>J. J. Palacios, A. J. Pérez-Jiménez, E. Louis, E. SanFabián, and J. A. Vergés, *Phys. Rev. B* **66**, 035322 (2002).
- <sup>13</sup>A. Pecchia and A. Di Carlo, *Rep. Prog. Phys.* **67**, 1497 (2004).
- <sup>14</sup>A. Prociuk, B. van Kuiken, and B. D. Dunietz, *J. Chem. Phys.* **125**, 204717 (2006).
- <sup>15</sup>A. R. Rocha, V. M. García-Suárez, S. Bailey, C. Lambert, J. Ferrer, and S. Sanvito, *Phys. Rev. B* **73**, 085414 (2006).
- <sup>16</sup>R. Landauer, *IBM J. Res. Dev.* **1**, 223 (1957).
- <sup>17</sup>See, e.g., Y. M. Blanter and M. Büttiker, *Phys. Rep.* **336**, 1 (2000); S. Camalet, J. Lehmann, S. Kohler, and P. Hänggi, *Phys. Rev. Lett.* **90**, 210602 (2003); Y. C. Chen and M. Di Ventra, *Phys. Rev. B* **67**, 153304 (2003); Y. C. Chen and M. Di Ventra, *Phys. Rev. Lett.* **95**, 166802 (2005); M. J. Montgomery *et al.*, *J. Phys.: Condens. Matter* **14**, 5377 (2002); Y. C. Chen, M. Zwolak, and M. Di Ventra, *Nano Lett.* **3**, 1691 (2003); R. D'Agosta, N. Sai, and M. Di Ventra, *ibid.* **6**, 2935 (2006); M. Di Ventra, S. J. Pantelides, and N. D. Lang, *Phys. Rev. Lett.* **88**, 046801 (2002); Z. Yang, M. Chohlou, M. Zwolak, Y. C. Chen, and M. Di Ventra, *Phys. Rev. B* **71**, 041402(R) (2005).
- <sup>18</sup>N. D. Lang, *Phys. Rev. B* **36**, 8173 (1987).
- <sup>19</sup>T. N. Todorov, *Philos. Mag.* **B 89**, 1577 (1999).
- <sup>20</sup>N. S. Wingreen, A.-P. Jauho, and Y. Meir, *Phys. Rev. B* **48**, 8487 (1993).
- <sup>21</sup>M. Grifoni and P. Hänggi, *Phys. Rep.* **368**, 409 (1998).
- <sup>22</sup>M. Büttiker, *J. Low Temp. Phys.* **118**, 519 (2000).
- <sup>23</sup>M. Büttiker, H. Thomas, and A. Prêtre, *Phys. Lett. A* **180**, 364 (1993); *Phys. Rev. Lett.* **70**, 4114 (1993).
- <sup>24</sup>M. Büttiker, *Nuovo Cimento Soc. Ital. Fis., B* **B110**, 509 (1995); M. Büttiker, in *Quantum Dynamics and Submicron Structures*, edited by H. Cerdeira, G. Schon, and B. Kramer (Kluwer Academic Publishers, Dordrecht, 1995), pp. 657–672.
- <sup>25</sup>M. Di Ventra and T. N. Todorov, *J. Phys.: Condens. Matter* **16**, 8025 (2004).
- <sup>26</sup>R. Baer, T. Seideman, S. Ilani, and D. Neuhauser, *J. Chem. Phys.* **120**, 3387 (2004).
- <sup>27</sup>G. Stefanucci and C.-O. Almbladh, *Phys. Rev. B* **69**, 195318 (2004).
- <sup>28</sup>A. P. Horsfield, D. R. Bowler, A. J. Fisher, T. N. Todorov, and C. G. Sánchez, *J. Phys.: Condens. Matter* **16**, 8251 (2004).
- <sup>29</sup>S. Kurth, G. Stefanucci, C.-O. Almbladh, A. Rubio, and E. K. U. Gross, *Phys. Rev. B* **72**, 035308 (2005).
- <sup>30</sup>N. Bushong, N. Sai, and M. Di Ventra, *Nano Lett.* **5**, 2569 (2005).
- <sup>31</sup>K. Burke, R. Car, and R. Gebauer, *Phys. Rev. Lett.* **94**, 146803 (2005).
- <sup>32</sup>Y. Zhu, J. Maciejko, T. Ji, H. Guo, and J. Wang, *Phys. Rev. B* **71**, 075317 (2005).
- <sup>33</sup>J. N. Pedersen and A. Wacker, *Phys. Rev. B* **72**, 195330 (2005).
- <sup>34</sup>X. Qian, J. Li, X. Lin, and S. Yip, *Phys. Rev. B* **73**, 035408 (2006).
- <sup>35</sup>C. G. Sánchez, M. Stamenova, S. Sanvito, D. R. Bowler, A. P. Horsfield, and T. N. Todorov, *J. Chem. Phys.* **124**, 214708 (2006).
- <sup>36</sup>E. Runge and E. K. U. Gross, *Phys. Rev. Lett.* **52**, 997 (1984).
- <sup>37</sup>N. Sai, M. Zwolak, G. Vignale, and M. Di Ventra, *Phys. Rev. Lett.* **94**, 186810 (2005).
- <sup>38</sup>M. Koentopp, K. Burke, and F. Evers, *Phys. Rev. B* **73**, 121403(R) (2006).
- <sup>39</sup>P. Bokes, J. Jung, and R. W. Godby, *cond-mat/0604317* (to be published).
- <sup>40</sup>P. Delaney and J. C. Greer, *Phys. Rev. Lett.* **93**, 036805 (2004).
- <sup>41</sup>S.-H. Ke, H. U. Baranger, and W. Yang, *cond-mat/0609637* (to be published).
- <sup>42</sup>C. Toher, A. Filippetti, S. Sanvito, and K. Burke, *Phys. Rev. Lett.* **95**, 146402 (2005).
- <sup>43</sup>B. Muralidharan, A. W. Ghosh, and S. Datta, *Phys. Rev. B* **73**, 155410 (2006).
- <sup>44</sup>G. Stefanucci, *cond-mat/0608401* (to be published).
- <sup>45</sup>C.-L. Cheng, J. S. Evans, and T. V. Voorhis, *Phys. Rev. B* **74**, 155112 (2006).
- <sup>46</sup>We have modified the SOCORRO code in order to include evolution in time (<http://dft.sandia.gov/Socorro/mainpage.html>).
- <sup>47</sup>R. W. Hockney, in *Methods in Computational Physics*, edited by B. Alder, S. Ferbach, and M. Rotenberg (Academic, New York, 1970), Vol. 9, p. 135.
- <sup>48</sup>G. Vignale and W. Kohn, *Phys. Rev. Lett.* **77**, 2037 (1996).
- <sup>49</sup>N. Bushong, J. Gamble, and M. Di Ventra (unpublished).
- <sup>50</sup>N. D. Lang and M. Di Ventra, *Phys. Rev. B* **68**, 157301 (2003).
- <sup>51</sup>M. Di Ventra and N. D. Lang, *Phys. Rev. B* **65**, 045402 (2002).
- <sup>52</sup>Note that a quasi-steady-state may not occur in a nanoscale junction, even in the presence of this fast momentum relaxation mechanism, if nonlaminar flow (like the one we observe in this work) occurs (see also Ref. 49).
- <sup>53</sup>P. C. Martin and J. Schwinger, *Phys. Rev.* **115**, 1342 (1959).
- <sup>54</sup>I. Tokatly and O. Pankratov, *Phys. Rev. B* **60**, 15550 (1999); I. V. Tokatly, *ibid.* **71**, 165104 (2005).
- <sup>55</sup>R. D'Agosta and M. Di Ventra, *J. Phys.: Condens. Matter* **18**, 11059 (2006).
- <sup>56</sup>S. Conti and G. Vignale, *Phys. Rev. B* **60**, 7966 (1999).
- <sup>57</sup>Note that in practical calculations, the electron liquid can have a nonvanishing numerical viscosity due to the discrete grid spacing.
- <sup>58</sup>N. Agrait, A. L. Yeyati, and J. M. van Ruitenbeek, *Phys. Rep.* **377**, 81 (2003).
- <sup>59</sup>The nonuniformity of the density of streamlines is partially due to the fact that we have calculated the streamlines using random initial points. The lines become denser when two or more initial points belong to nearby streamlines.

- <sup>60</sup>K.-F. Berggren, A. F. Sadreev, and A. A. Starikov, *Phys. Rev. E* **66**, 016218 (2002).
- <sup>61</sup>I. V. Zozoulenko and T. Blomquist, *Phys. Rev. B* **67**, 085320 (2003).
- <sup>62</sup>L. D. Landau and E. M. Lifshitz, *Fluid Mechanics*, 2nd ed., Course of Theoretical Physics, Vol. 6 (Pergamon, New York, 1987).
- <sup>63</sup>H. Mera, P. Bokes, and R. W. Godby, *Phys. Rev. B* **72**, 085311 (2005).
- <sup>64</sup>G. F. Giuliani and G. Vignale, *Quantum Theory of the Electron Liquid*, 1st ed. (Cambridge University Press, Cambridge, 2005).
- <sup>65</sup>Including the exchange and correlation effects reduces the pressure slightly compared to the noninteracting results (Ref. 64).
- <sup>66</sup>G. Vignale, C. A. Ullrich, and S. Conti, *Phys. Rev. Lett.* **79**, 4878 (1997).
- <sup>67</sup>D. R. Hamann, *Phys. Rev. B* **40**, 2980 (1989).
- <sup>68</sup>J. P. Perdew and A. Zunger, *Phys. Rev. B* **23**, 5048 (1981).
- <sup>69</sup>H. Tal-Ezer and R. Kosloff, *J. Chem. Phys.* **81**, 3967 (1984).